Computer Simulation of Modulated Structures and Diffuse Scattering in *B*8-type (Co, Ni, Cu)$_{1+x}$(Ge, Sn) Phases

Andrew G. Christy and Ann-Kristin Larsson

Research School of Chemistry, Australian National University, G.P.O. Box 414, Canberra, ACT 2601, Australia

The compounds (Co, Ni)(Ge, Sn) and Cu$_{1+x}$ have hexagonal average structures intermediate between those of NiAs and Ni$_2$In. Ordering of atoms and vacancies in the partially occupied A' sites produces a variety of superstructures of lower symmetry. In the structures of this study, the modulation vector is always in the (*hhl*) plane. Diffuse scattering observed in some cases implies the occurrence of short-range order only. The effect of two-site interactions on determining the preferred long-range and short-range ordering patterns was investigated by using a Monte Carlo simulation technique to generate two-dimensional arrays of "atoms" and "vacancies" and calculating the corresponding scattering patterns. It is shown that many of the 18 symmetrically distinct first- and second-nearest-neighbor interaction energies are nonzero in these systems but that the preferred ordering pattern is in most cases determined by variation in only three second-nearest-neighbor terms. These three parameters vary with both composition and temperature. The undulating diffuse streaks observed in electron diffraction in the Sn-bearing and Co–Ge systems are shown to arise from a combination of negligible interactions along z, strong interactions in the xy plane, and weak diagonal interactions. © 1998 Academic Press

INTRODUCTION

A great many $A_{1+x}B$ intermetallic phases are known whose average structure is intermediate between those of NiAs (*B*8$_1$) and Ni$_2$In (*B*8$_2$). Both semiconductor ($c/a \gg 1$) and metallic ($c/a = 1.2–1.3$) examples are known. In most cases, there is formation of one of a wide range of superstructures by ordering of vacancies and the additional cations interstitial to the NiAs substructure: 23 such examples are discussed in Lidin and Larsson (1). This study is concerned with a well-defined subset of these compounds including those of Cu–Sn, which are of technological importance due to their occurrence in bronzes, solders, and alloys such as Babbitt metal (2). The compounds of this study share the simplifying structural feature that there is no modulation of the structure down the direction [1$\bar{1}$0]; therefore, the ordering patterns can be treated reasonably comprehensively in two-dimensional projection normal to

[1$\bar{1}$0]. Note that all crystallographic directions and Miller indices will be expressed in terms of the NiAs/Ni$_2$In subcell with $b \approx 4$ Å and $c \approx 5$ Å unless stated otherwise. The systems studied (Co–Sn, Ni–Sn, Cu–Sn, Co–Ge, Ni–Ge) show electron diffraction evidence of eight different commensurate superstructures and also exhibit diffuse scattering due to short-range order, but it is shown that all of these scattering features can be simulated at least qualitatively in diffraction patterns calculated from a two-dimensional model with relatively straightforward variation in the interaction energies between the partially occupied sites.

In the *B*8-type average structure of these alloys, there are three symmetrically distinct sites, which we may label, A, A', and B. The A' site is vacant in NiAs, fully occupied by Ni(2) in Ni$_2$In, and partially occupied in the compounds of this study. Site A corresponds to the Ni of NiAs or the Ni(1) of Ni$_2$In. The A atoms are octahedrally coordinated by B, and the AB_6 octahedra form continuous edge-sharing sheets parallel to (001), as seen in Fig. 1a. In the average structure, all octahedra in any given (001) layer are translationally equivalent. Along the **z** direction, the octahedra share faces with those of adjacent layers, as seen in Fig. 1b, where the structure is viewed down [1$\bar{1}$0]. Between groups of three octahedra in one layer and the three in the adjacent layer lie "trigonal bipyramidal" interstices containing the A' sites. The full coordination of the A' atom when it is present includes not just the five B atoms forming the trigonal pyramid but also the trigonal prism formed by the six neighbouring A atoms, giving an overall coordination number of 11. The polyhedron formed by all 11 neighbors of the A' atom is that described by Edshammar (3). Dashed lines in Figs. 1a and 1b indicate the positions of Edshammar polyhedra relative to the AB_6 octahedra.

An alternative description of the structure that is more useful for the purposes of this study is as a continuous space-filling of Edshammar polyhedra. Figure 1c shows that these form continuous face-sharing (001) layers, whereas the view down [1$\bar{1}$0] (Fig. 1d) shows that the Edshammar polyhedra share vertices along **z** to form open (1$\bar{1}$0) layers. Adjacent layers share oblique faces so as to fill space completely. When all layers are superposed, the resulting pattern
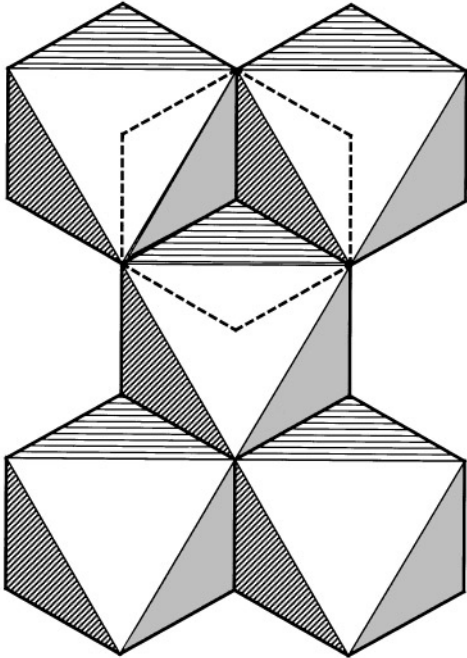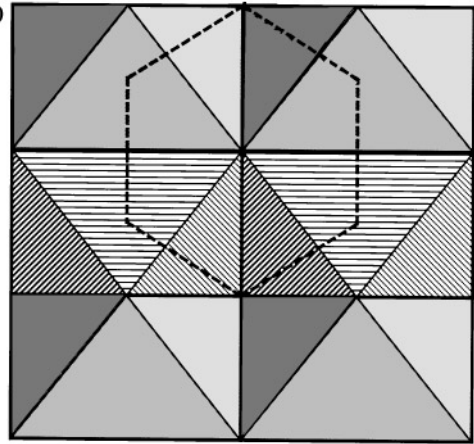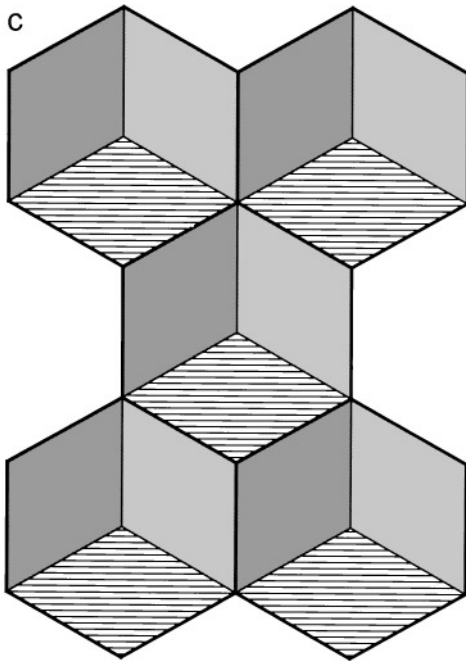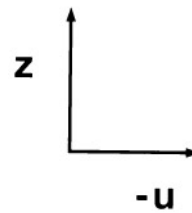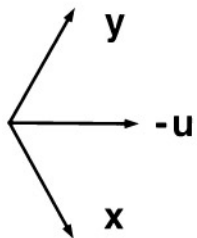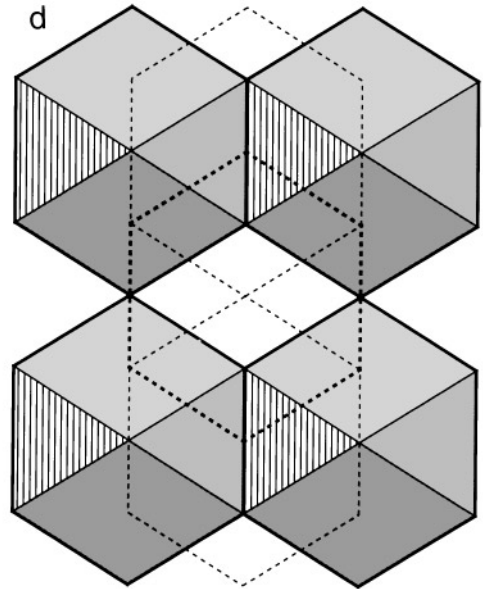
formed by the A' sites in this projection is a rectangular net with repeats $a/2$ and $c/2$. This representation of the structure will be used herein in describing A' occupancy patterns.

The detailed linkage pattern of the Edshammar polyhedra is as follows:

(i) Each A' coordination polyhedron shares triangular faces with six others in a hexagon along $\langle 100 \rangle$ vectors.

(ii) Each polyhedron shares rhomboidal faces with six others along $\langle \frac{1}{3}, \frac{2}{3}, \frac{1}{2} \rangle$ vectors, forming a trigonal prism.

(iii) Each shares a single corner with six others along $\langle \frac{4}{3}, \frac{2}{3}, \frac{1}{2} \rangle$ vectors, which form a large trigonal prism around the central atom.

(iv) Each shares a single corner with two others above and below along $\langle 001 \rangle$.

Each Edshammar polyhedron is therefore linked to a total of 20 others through the A and B atoms, 12 through face-sharing and 8 through corner-sharing.

Structure refinement of η'-Cu$_6$Sn$_5$ (4) shows that there is significant local strain associated with occupation of the A' site by Cu. Relative to vacant sites, the Sn atoms at $\pm \mathbf{z}/2$ are moved away by 0.2 Å, the three equatorial Sn are moved away by 0.15 Å, and the six Cu neighbors (in three symmetrically distinct sets) are moved inward by 0–0.1 Å. The net result is to make the Edshammar polyhedron both larger and more regular, bringing all 11 distances within 2.60–2.74 Å rather than the range 2.41–2.72 Å expected if the atoms were not displaced off their ideal $B8$ positions. The displacement is substantial and readily provides a rationale for correlation of occupancy between nearby Edshammar polyhedra. For instance, occupation of two A' sites related along $[001]_{B8}$ would require contraction of the bonds on both sides of the shared B atom; the A' atoms would therefore tend to contract in toward this central B atom, and the strain would propagate further than if one A' site were vacant. This relative positioning of occupied A' sites would be expected to be energetically unfavorable and little observed. This is in fact the case in the structures studied. Similarly, near-neighbor A' atoms tend to avoid clustering in the $\mathbf{xy}$ plane. In this study, it is shown that the distributions of A' atoms and vacancies that are consistent with the observed diffraction behavior are consistent with the existence of significant interactions between A' sites out to second-nearest neighbors as defined by face- or corner-sharing, i.e., distances of at least 9 Å in the $\mathbf{xy}$ plane and 10 Å along $\mathbf{z}$.

Although the local atomic displacements are clearly important in optimizing the local coordination geometry and in causing preferential occupation and avoidance of particular A' sites, it is unlikely that correlated displacements propagate very far. This is because the displacement field around any given A' atom is complicated in its geometry–at least octupolar, with local expansion of the structure both parallel and perpendicular to $\mathbf{z}$, and contraction at intermediate azimuthal angles. Therefore, only the scattering due to occupancy of the A' sites is considered in this paper. It will be seen that this suffices to reproduce the observed diffraction patterns reasonably well.

For systems where the $x = 0$ and $x = 1$ compositions have been observed, it should be noted that two-phase regions separate these compositions from intermediate solid solutions. Furthermore, strong displacive modulations occur in the $x = 0$ and $x = 1$ phases that are not observed in those of intermediate composition. Therefore, the end-member compositions are not considered in this study.

EXPERIMENTAL DIFFRACTION BEHAVIOR

The various superstructures observed in these systems are described in detail elsewhere (5, 6). A brief summary is provided here for reference. Given the lack of modulation of the structure down $[1\bar{1}0]$, only the $h\,h\,l$ diffraction patterns are described. These all contain a rectangular net of sublattice Bragg peaks at $(h\,h\,2l)$ and a wide variety of more diffuse superlattice maxima and streaks. The A' ordering patterns of the various commensurate superstructures may be seen in a simple, diagrammatic form projected down $[1\bar{1}0]$ in Fig. 2.

Co–Ge System

Diffraction patterns were obtained from compositions estimated as $x = 0.63$–0.86. Nearly continuous curved streaks of diffuse scattering were observed, which passed through intensity maxima close to $(0.33\,0.33\,0.5)$ and through positions of maximum $h = h_1$ at $(h_1\,h_1\,0)$ and $(h_1\,h_1\,2)$ and of minimum $h = h_2$ at $(h_2\,h_2\,1)$. The amplitude of the sinusoidal oscillation increased with x. For $x = 0.63$, $h_1 = 0.35$ and $h_2 = 0.30$, whereas for $x = 0.86$, $h_1 = 0.50$ and $h_2 = 0.25$.

Co–Sn System

The Co–Sn system has been examined over the range $x = 0.38$–0.63 quenched from 1000°C (4). Sharp superlattice spots at $(0.25\,0.25\,1)$ and $(0.75\,0.75\,1)$ in slowly cooled material correspond to the ordering pattern of γ'-Co$_3$Sn$_2$ (7, 8). Fast quenching produced sinusoidal streaks similar to those observed for the Co–Ge system. These streaks had intensity

FIG. 1. Portions of the structure of NiAs depicted conventionally as a space-filling of AB_6 octahedra viewed (a) down [001] and (b) along [1$\bar{1}$0]. The $\mathbf{z}$ axis is vertical in (b). The positions of Edshammar polyhedra centered on A' sites, A' (A_6B_5), are indicated by dashed lines. An alternative depiction of the structure as a space-filling of Edshammar polyhedra is shown viewed down [001] in (c) and down [1$\bar{1}$0] in (d). The positions of polyhedra in the next two layers are shown dashed in (d). Axes for the $B8$ substructure are indicated in (c) and (d).
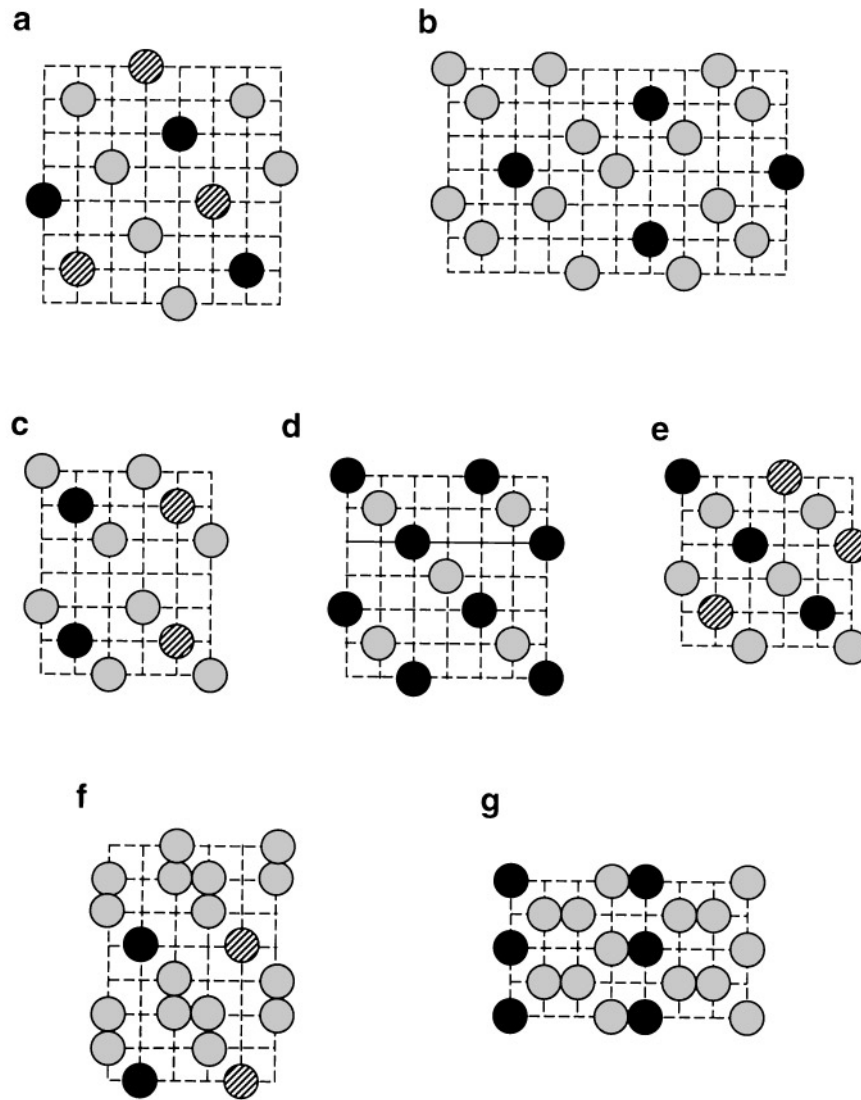
FIG. 2. The commensurate superstructures found in the Cu–Sn, Ni–Ge, and Co–Sn systems, projected down $[1\bar{1}0]$. The **z** axis is vertical. Circles indicate minority constituents, which may be atoms or vacancies. A set of translationally equivalent sites is highlighted black at height zero and shaded at $\frac{1}{2}t_{[1\bar{1}0]}$. (a) η'-Cu_6Sn_5, (b) η^8-Cu_5Sn_4, (c) η^6-Cu_5Sn_4, (d) γ^4-$Ni_{17}Ge_4$, (e) Ni_5Ge_3, (f) $Ni_{17}Ge_{12}$ or $Ni_{19}Ge_{12}$, (g) γ'-Co_3Sn_2.

maxima near the (0.25 0.25 1) position and crossed the $l = 0$ plane near (0.33 0.33 0).

Ni–Ge System

This is the most complex of the systems studied. Compositions synthesized range from $x = 0.33$ to $x = 1.00$. Over that composition range, several different types of diffraction behavior are seen. The boundaries between these diffraction regimes are temperature dependent; composition ranges given here are for quenches from about 700°C.

(i) $x = 0.33$: The scattering is weak and diffuse, difficult to interpret, and may be similar to that of the Co–Sn system.

(ii.a) $x = 0.41–0.50$: Strong modulation spots appear at (0.33 0.33 0.50) on faint streaks parallel to **z***. Second-order spots at (0.33 0.33 1) and higher orders may also be visible.

(ii.b) $x = 0.58$: The (0.33 0.33 0.5) spots are strongly elongated along **z***. The modulation vector of (ii.a,b) corresponds to the broad $Ni_{17}Ge_{12}$–$Ni_{19}Ge_{12}$ field of ref 6.

(iii) $x = 0.63–0.67$: The spots have moved to (0.33 0.33 0.33) with strong second-order spots at (0.33 0.33 0.67). This is the Ni_5Ge_3 field of ref 6.

(iv) $x = 0.70$: Broad spots are measured at (0.31 0.31 0.50). These are elongated along curved streaks that pass through (0.50 0.50 0) like those in the Co–Ge system.

(v) $x = 0.75$: Two sets of modulations are measured at $(0.36\,0.36\,0.54)$ and $(0.27\,0.27\,0.54)$. These both lie on curved streaks like those of Co–Ge. Two phases of different structure but similar composition are likely (6).

(vi) $x = 0.78$: Complex, faint diffuse scattering is observed. Diffuse maxima at about $(0.25\,0.25\,0.58)$ lie on curved streaks that have manimum h at $(0.15\,0.15\,1)$.

(vii) $x = 0.87$: Modulation spots are measured at $(0.5\,0.5\,0)$ and (001). Faint streaks possible interconnect these, or may be related to those of (vi). The spots appear to correspond to the displacive modulation of Ni$_2$Ge, suggesting that there are two phases present, one of which has the distorted structure known for $x = 1$.

The diffuse maxima are usually close to or exactly at commensurate positions. The corresponding supercells always have a period along **y** and **z** that is tripled or quadrupled relative to the projected $a/2$ and $c/2$ periods of the B8 subcell. Structure solutions for superstructures in this system were obtained by Ellner *et al.* (9) in the case of $x = 0.58$ (Ni$_{19}$Ge$_{12}$) and $x = 0.67$ (Ni$_5$Ge$_3$). In the structures of Ellner, interstitials occupied either $\frac{1}{3}$ or $\frac{2}{3}$ of each (001) layer of A' sites such that the majority constituents formed a honeycomb pattern; the same occupation pattern for (001) layers is found in the η^6-Cu$_5$Sn$_4$ structure. The honeycomb ordering principle is easily extrapolated to construct a model structure for Ni$_{17}$Ge$_{12}$ by exchanging the occupied and vacant sites of Ni$_{19}$Ge$_{12}$, which has the same modulation vector. This structure is herein interchangeably designated Ni$_{17}$Ge$_{12}$, Ni$_{19}$Ge$_{12}$, or Ni$_{17-19}$Ge$_{12}$. Any composition between $x = 0.333$ and $x = 0.667$ can be obtained by appropriate combinations of honeycomb layers.

A unit cell and space group for $x = 0.75$ (γ^4-Ni$_{17}$Ge$_4$) were proposed by Brand (7) from X-ray powder data. The ordering pattern deduced by Larsson and Withers (6) is the only one that fits Brand's unit cell and that necessarily has monoclinic symmetry or below. This structure was not observed experimentally by Larsson and Withers since a complex diffraction pattern with two sets of sinusoidal streaks was obtained at this composition. Nevertheless, the γ^4 structure was simulated satisfactorily in this study.

Ni–Sn System

Diffraction was observed from a range of compositions with $x = 0.34$–0.61 quenched from 900°C (5). Diffuse maxima occurred at $(h_1 h_1 0)$ and $(h_2 h_2 1)$ positions rather than at $l = 0.5, 1.5$ as seen in the Ni–Ge system. The maxima were connected by streaks undulating along the **z*** direction. As in the Co–Ge system, the amplitude of the undulations decreased with increasing x. For $x = 0.34$, $h_1 = 0.40$ and $h_2 = 0.21$, whereas for $x = 0.61$, $h_1 = 0.35$ and $h_2 = 0.27$. The $(h_2 h_2 1)$ spots are close in position to the superlattice maxima in γ'-Co$_3$Sn$_2$.

Cu–Sn System

The B8 substructure exists over a narrow composition range with $x = 0.20$–0.30. The lower x compositions are stable at lower temperature and show an ordered superstructure (η'-Cu$_6$Sn$_5$) with modulation spots at $(0.40\,0.40\,0.40)$ and $(0.20\,0.20\,0.80)$, whereas at larger x and higher temperature, two superstructures corresponding to $5:4$ stoichiometry are found: the η^6 structure with reflections at $(0.33\,0.33\,0.50)$ and the η^8 structure with spots at $(0.375\,0.375\,0.50)$ and second-order spots at $(0.25\,0.25\,1)$. The η^6 structure appears to be stable at higher temperature than η^8, but the two may coexist (10).

INTERACTIONS BETWEEN A' SITES

The correlation in occupancy between two neighboring sites separated by a given vector in a structure can be expressed in several ways. Perhaps the simplest is to express the distribution of atoms between the sites as an equilibrium constant:

$$K = 4(N_{VV} N_{OO})/(N_{VO})^2$$

where $N_{VV} = $ the total number of vacant–vacant pairs, $N_{OO} = $ the number of doubly occupied pairs, and $N_{VO} = $ the number of occupied–vacant pairs. If there is no energetic preference for any of these configurations, $K = 1$. If $K > 1$, doubly occupied and/or doubly vacant pairs are preferred. If $K < 1$, the two sites show a preference for unequal occupancy. The constant K can be calculated for each set of symmetry-related vectors between A' sites and may be converted into a corresponding free energy expressed in units of kT ($k = $ Boltzmann constant, $T = $ absolute temperature) by the relation $G/kT = -\ln K$. Note that replacing vacant sites by occupied sites and vice versa gives a structure with exactly the same interaction energies but composition $1 - x$ rather than x. Apparent interaction energies obtained in this way, from observed atomic configurations, will be termed C_{ij} in this study.

In the simulation work of this study, the A' sublattice is projected down $[1\bar{1}0]$ to give a two-dimensional rectangular net with translation vectors $(\mathbf{x} + \mathbf{y})/2$ and $\mathbf{z}/2$. Equilibrium constants and interaction energies are then calculated for vector sets ($\pm i \times (\mathbf{x} + \mathbf{y})/2$, $\pm j \times \mathbf{z}/2$) where $i, j \geq 0$. All energies for different (i, j) are assumed to be independent. It should be noted that the hexagonal symmetry of the B8 substructure is not maintained. This is reasonable since although there is strong positive correlation between occupancies along the projection direction, *negative* correlations are observed in directions related to this by the hexad of the average structure. We deduce that mutually frustrating repulsive interactions along three directions at 120° to one another force symmetry–breaking in these systems. An advantage of assuming the symmetry-breaking as given is that

TABLE 1
Apparent Interaction Energies C_{ij} for Known Commensurate Superstructure

ij	Ideal x and example						
	0.20, 0.80 η'-Cu$_6$Sn$_5$	0.25, 0.75 η^6-Cu$_5$Sn$_4$	0.25, 0.75 η^8-Cu$_5$Sn$_4$	0.25, 0.75 γ^4-Ni$_7$Ge$_4$	0.33, 0.67 Ni$_5$Ge$_3$	0.42, 0.58 Ni$_{19}$Ge$_{12}$	0.50 γ'-Co$_3$Sn$_2$
01	$+\infty$	$+\infty$	$+\infty$	$+\infty$	$+\infty$	$+0.12$	$+\infty$
02	$+\infty$	$+\infty$	$+\infty$	$+\infty$	$+\infty$	$+\infty$	$+\infty$
03	$+\infty$	$+\infty$	$+\infty$	$+\infty$	$-\infty$	$+0.12$	$+\infty$
04	$+\infty$	$-\infty$	$-\infty$	$-\infty$	$+\infty$	$-\infty$	$-\infty$
10	$+\infty$	$+\infty$	$+\infty$	$+\infty$	$+\infty$	$+1.67$	0
11	$+\infty$	-0.56	0	-1.61	-1.10	$+0.12$	0
12	-1.95	-0.56	-1.61	$+\infty$	-1.10	-1.32	0
13	-1.95	-0.56	0	-1.61	$+\infty$	$+0.12$	0
20	$+\infty$	$+\infty$	$+\infty$	$+\infty$	$+\infty$	$+1.67$	$+\infty$
21	-1.95	-0.56	-1.61	$+\infty$	-1.10	$+0.12$	$-\infty$
22	$+\infty$	-0.56	$+\infty$	$-\infty$	-1.10	-1.32	$+\infty$
23	$+\infty$	-0.56	-1.61	$+\infty$	$+\infty$	$+0.12$	$-\infty$
30	$+\infty$	$-\infty$	-1.61	$+\infty$	$-\infty$	$-\infty$	0
31	-1.95	$+\infty$	0	-1.61	$+\infty$	$+0.12$	0
32	$+\infty$	$+\infty$	$+\infty$	$+\infty$	$+\infty$	$+\infty$	0
40	$+\infty$	$+\infty$	$+\infty$	$-\infty$	$+\infty$	$+1.67$	$-\infty$
41	$+\infty$	-0.56	$+\infty$	$+\infty$	-1.10	$+0.12$	$+\infty$
42	-1.95	-0.56	$-\infty$	$+\infty$	-1.10	-1.32	$-\infty$

this restricts the number of twin orientations available in the simulations, increases the average size of any given domain, and aids recognition of superstructures since the direction common to all of them is always parallel to the projection line.

Although the interaction energies obtained are useful for characterizing observed and calculated structures, it should be noted that they are only qualitative indicators of the correlations in the three-dimensional structure. Two-dimensional interaction energies C_{ij} are given in Table 1 for the commensurate superstructures of Fig. 2. Note that energies obtained in this way, for fully ordered structures, are always either $+\infty$, $-\infty$, or a small number (magnitude <2.0).

SIMULATION

The computer model used in this work filled a given proportion x of the interstitial sites in a 500×500 array with cations. There is an energy of interaction E between each site (y, z) and its neighbors $(y \pm i, z \pm j)$ such that $E = E_{ij}$ if both sites are vacant or both are occupied and $E = -E_{ij}$ if one is occupied and the other is not. The E_{ij} values were input at the start of the run and are distinct from energies C_{ij} calculated from the final interstitial distribution, although the two quantities showed good qualitative agreement (see later). Hexagonal symmetry, which would relate $(i, j) = (0, 1)$ and $(1, 1)$, $(1, 0)$ and $(2, 0)$, etc., was not assumed. Vacancies and interstitials were exchanged until the energy was minimized using a Monte Carlo strategy. In a single

cycle, a vacant site and an occupied site were picked at random and their interaction energies evaluated. They were swapped automatically if to do so was energetically favorable, and with only a small probability if it was not. A total of 12 million such trials were made, so each site was examined an average of 48 times. Typically, 90% of the observed energy reduction was achieved in the first 2,000,000 trials, and another 5% in the next 2,000,000. Only 0.3% decrease in energy was seen during the last 1,000,000 cycles. Clearly, the final atomic distributions were not fully equilibrated but were reasonably close. The configurations obtained were output as image files and also as a list of C_{ij} calculated from the observed equilibrium constants. These empirical interaction energies were only qualitatively related to the E_{ij} values input, partly due to imperfect equilibrium and partly due to complex coupling between different interactions, so that a given E_{ij} interaction affected occupancy correlations for a wide range of different (i, j). Although i and j may take arbitrarily large values, corresponding to very long-range interactions, it was found in practice that interactions beyond next-nearest neighbor had a negligible effect on the calculated C_{ij} energies, so only interactions with first- and second-nearest neighbors were considered. There are 18 such symmerically distinct (i, j) pairs in total. The corresponding (i, j) pairs are shown in Fig. 3.

C_{ij} values larger in magnitude than 4 were only rarely obtained, irrespective of the size of the E_{ij} terms, so the working maximum E_{ij} magnitude used in the final simulations was 5.
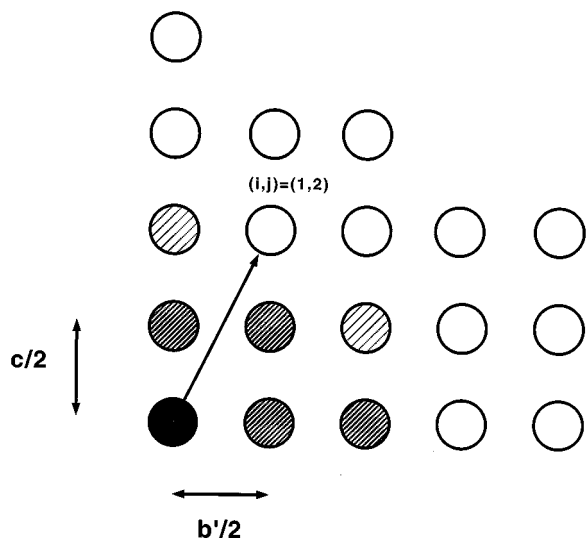
FIG. 3. First- and second-nearest-neighbor A' sites relative to the origin (black) in $[1\bar{1}0]$ projection. The vector for the E_{12} interaction is also shown. First-nearest neighbors by face-sharing are shaded darkly, first-nearest neighbors by corner-sharing are shaded lightly, and second-nearest neighbors are unshaded.

TABLE 2
E_{ij} Terms Used to Calculate Occupancy Patterns and Corresponding Diffraction Patterns[a]

ij	Normal	η'-Cu$_6$Sn$_5$	Ni$_{17-19}$Ge$_{12}$	Fig. 9a	Fig. 9b
10	+5	+5	+5	+5	+5
20	+5	+5	+5	+5	+5
30	var	+5	−5	0	0
40	+5	+5	+5	0	0
01	+5	+5	0	+1	0
11	0	+5	0	0	0
21	0	0	0	−1	−2
31	0	0	0	−1	−1
41	+5	+5	0	0	0
02	+5	+5	+5	+1	+1
12	0	0	0	0	0
22	var	+5	0	0	0
32	+5	+5	+5	0	0
42	−5	0	0	0	0
03	+5	+5	0	0	0
13	0	0	0	0	0
23	var	+5	0	0	0
04	−5	+5	−5	0	0

[a] Values from Column were used to produce Figs. 4–6 and 8. Columns 3–6 show values used to produce Figs. 7 and 9.

RESULTS

Commensurate Superstructures

Diffraction patterns were calculated from the output files using the program DIFFUSE, which employs the algorithm described in ref. 11, running on the Fujitsu vpp300 supercomputer. As can be seen from Table 1, several C_{ij} terms maintain consistent values in all or most of the commensurate structures. Therefore, initial attempts to simulate the ordered superstructures were made with E_{ij} set to the values shown in Table 2. Note in particular that E_{10}, E_{20}, E_{01}, and E_{02} always tend to be large positive, implying that it is not favorable for first-nearest-neighbor sites in the **xy** plane or along **z** to be of the same occupancy. Since occupancy of the A' sites causes expansion of the site, the signs of these terms presumably arise from the need to avoid strain accumulation, which favors vacant sites as nearest neighbors of occupied ones.

In general, only the three parameters E_{22}, E_{23}, and E_{30} were important in determining the type of ordering. Values taken by these terms for the different superstructures are set out in Table 3. A great simplification of the parameter space was achieved since the number of variable parameters was reduced from 18 to 3. The **xy** parameters E_{10}, E_{20}, and E_{40} and those parallel to **z**, E_{01}–E_{03}, were all set at the values $+5$. E_{30} was varied: for those structures in which the minority A' species form a honeycomb pattern in (001) layers, it was negative ($E_{30} = -5$); otherwise, it was positive ($E_{30} = +5$). If the adjustable parameters E_{22}, E_{23}, and E_{30} were all left equal to zero, a simple incommensurate

modulated pattern was obtained, showing only first-order modulation spots at $(\pm k, k \pm l)$ where $k \approx \frac{1}{3}$ and $l \approx \frac{1}{2}$. The values of these indices were found to be very sensitive to the magnitudes of the E_{i0} and E_{0j} parameters, respectively.

The calculated real space occupancy patterns using only the three variable parameters E_{22}, E_{23}, and E_{30} were satisfactory for five out of seven of the commensurate superstructures examined. Even in the few instances when a fixed E_{ij} parameter had the opposite sign to the C_{ij} of the ideal structure, such as E_{02} for γ'-Co$_3$Sn$_2$, the stability field of the structure in parameter space was evidently large enough for it to grow nevertheless, as can be seen from the lattice realization ("image") and diffraction pattern of Fig. 4. Note that the program DIFFUSE subtracts Bragg scattering from the average structure. Ideally, the substrate Bragg

TABLE 3
Settings of E_{22}, E_{23}, and E_{30}, Required for Superstructures of Figs. 4–6 and 8

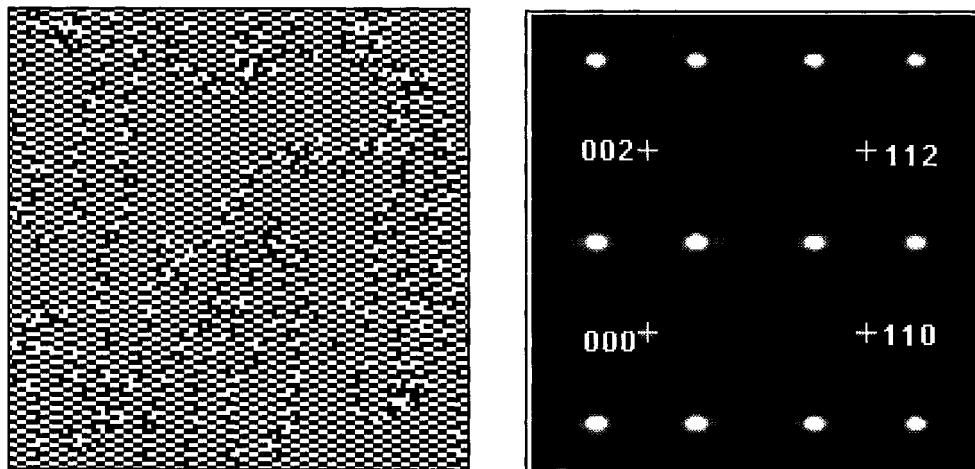| Structure	E_{22}	E_{23}	E_{30}
η'-Cu$_6$Sn$_5$	+5	+5	+5
η^6-Cu$_5$Sn$_4$	0	0	−5
η^8-Cu$_5$Sn$_4$	0	+5	0
γ^4-Ni$_7$Ge$_4$	+5	−5	+5
Ni$_5$Ge$_3$	+5	0	−5
Ni$_{17-19}$Ge$_{12}$	0	0	−5
γ'-Co$_3$Sn$_2$	−5	+5	0

FIG. 4. Portions of calculated image (left) and diffraction pattern (right) for γ'-Co_3Sn_2. Each pixel in the image represents a column A' projected down $[1\bar{1}0]$, either fully occupied (black) or vacant (white). Only weak scattering is seen in the diffraction pattern at the positions of the substructure Bragg maxima, whose positions are indicated by crosses. Indices are for the $B8$ subcell.

reflections would be completely missing. In practice, fluctuations in the local average composition prevent the subtraction algorithm from removing them completely, and their positions are indicated by weak diffuse spots. These are highlighted by superimposed marks in Fig. 4. Crystallites of the target superstructures were observed of the order of 10 supercell repeats across in the better simulations, and the diffraction patterns resembled those of the fully ordered structures. The calculated images for these runs may be seen in Fig. 5, and corresponding diffraction patterns in Fig. 6.

In contrast to the "satisfactory" runs, the η'-Cu_6Sn_5 and $Ni_{17}Ge_{12}$ structures did not develop well with the same set of fixed E_{ij}. The real-space ordering pattern was highly disordered in the attempted simulation of the η' phase, whereas that obtained for the attempt at $Ni_{17}Ge_{12}$ showed exsolution into two phases with strongly negative C_{02} and $x = \frac{1}{3}$ and $x = \frac{1}{2}$, respectively. In both cases, the target structures could be more faithfully simulated if additional E_{ij} were changed. In the case of the η' structure, $E_{04} = -5$, $E_{11} = +5$, and $E_{42} = 0$ were all needed to give crystallites of the desired phase. The honeycomb layers of $Ni_{17-19}Ge_{12}$ were produced, albeit with many stacking faults, for $E_{01} = 0$, $E_{03} = 0$, $E_{41} = 0$, and $E_{42} = 0$. The negative C_{02} (-4.29) for the ordering pattern of Fig. 5f appeared to be driven by the positive E_{01} and E_{03} parameters and became strongly positive ($+4.58$) if these terms were set at zero. The improved real space and reciprocal space patterns for these ordering schemes may be seen in Fig. 7. The E_{ij} for the additional runs are set out in columns 3 and 4 of Table 3. It should be noted that the calculated real space ordering pattern is a much more sensitive indicator of the state of order than the diffraction pattern. As stated earlier, a dif-

fraction pattern calculated for E_{22}, E_{23}, and $E_{30} = 0$ gives strong first-order modulation spots at (0.33 0.33 0.5), where they would be expected for the $Ni_{17-19}Ge_{12}$ structure. However, no order is discernible in the real space pattern unless the appropriate E_{ij} are given nonzero values. The nonuniqueness of real space ordering patterns corresponding to a given modulation wave vector is an illustration of the phenomenon demonstrated by Welberry and Withers (12), where multisite correlations that have a strong effect on real space ordering patterns are evidenced in the phases but not the intensities of the corresponding diffraction pattern. In the absence of phase information, the diffraction pattern supplies information on only two-point correlations (corresponding in real space to the E_{ij} of this paper).

Correspondents to Superstructures at Different Compositions

The superstructures observed for the Cu–Sn alloys are not found in the Ni–Ge system, and this presumably correlates with the composition ranges of the two systems being quite distinct: 0.2–0.3 for Cu–Sn and approximately 0.4–0.8 for Ni–Ge. It is instructive to take the sets of E_{ij} parameters corresponding to the various Cu–Sn structures and apply them to compositions more typical of the Ni–Ge compounds. This provide a check on whether the intersite interactions are or are not significantly different in the two systems. Whereas some superstructures at $x = 0.25$ may be generated by sets of E_{ij} similar to those of $x = 0.5$ structures, but with less dense occupation of favorable sites, other ordering patterns may correspond to quite different E_{ij} values.
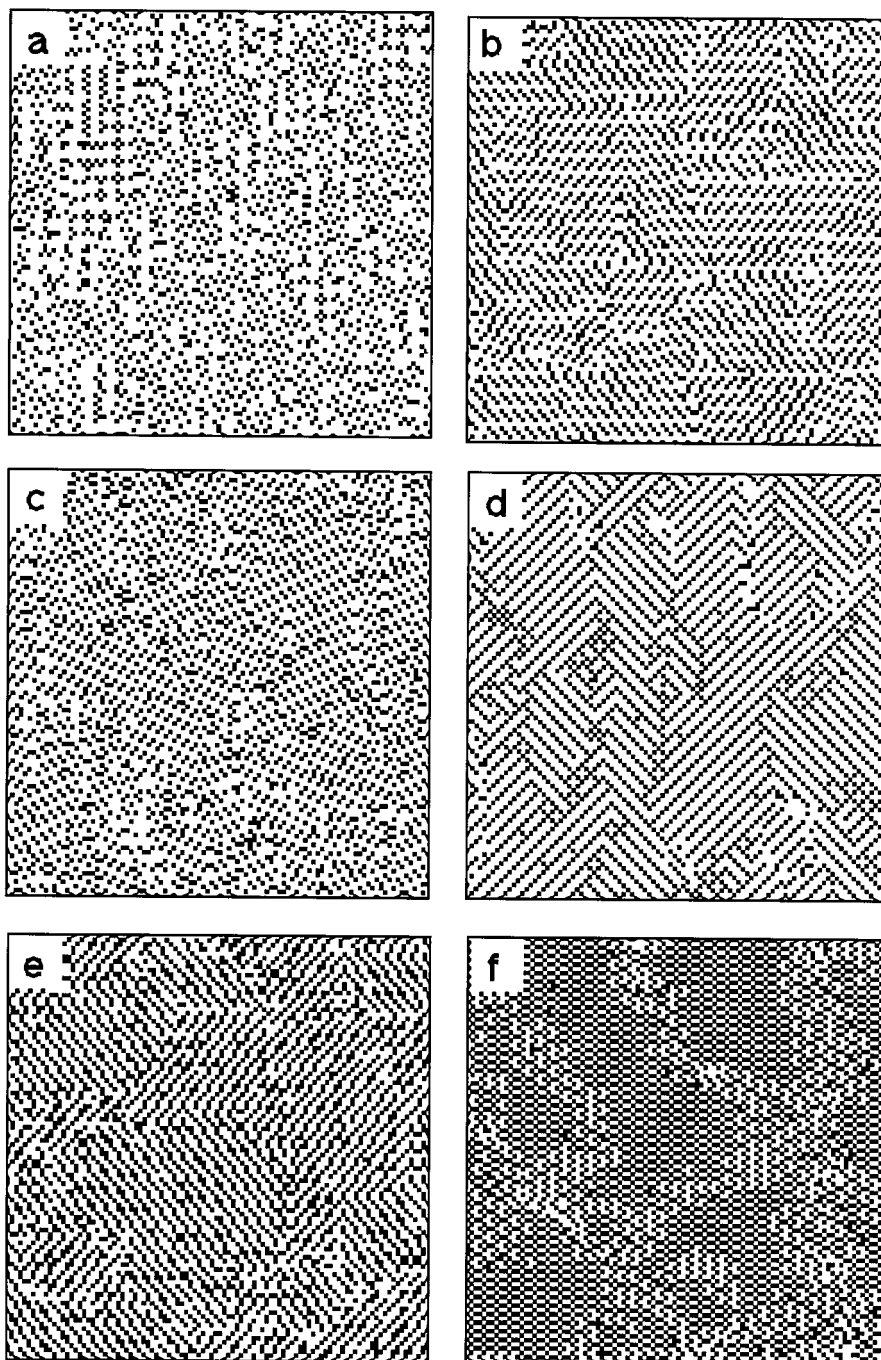
FIG. 5. Calculated "images" using the E_{ij} values from the second columns of Tables 2 and 3. (a) η'-Cu_6Sn_5, (b) η^6-Cu_5Sn_4, (c) η^8-Cu_5Sn_4, (d) γ^4-Ni_7Ge_4, (e) Ni_5Ge_3, (f) $Ni_{17}Ge_{12}$.

Some calculated real space ordering patterns are shown in Fig. 8. It can be seen that the E_{ij} used for both η^6 and η^8 phases give rise to multiphase mixtures at $x = 0.5$. For η^6, one of the phases has the $Ni_{17}Ge_{12}$ structure whereas the other is a second "honeycomb phase" with period $2c$ and $x = 0.5$. This second phase appears to be the same as that intergrown with $Ni_{17}Ge_{12}$ in the improved simulation of Fig. 7b. When the E_{ij} corresponding to the η^8 structure were used, both these structures were observed again, in somewhat more disordered form, but the predominant phase had the γ'-Co_3Sn_2 structure, as well-ordered crystallites. For comparison, patterns were also calculated for the E_{ij} of
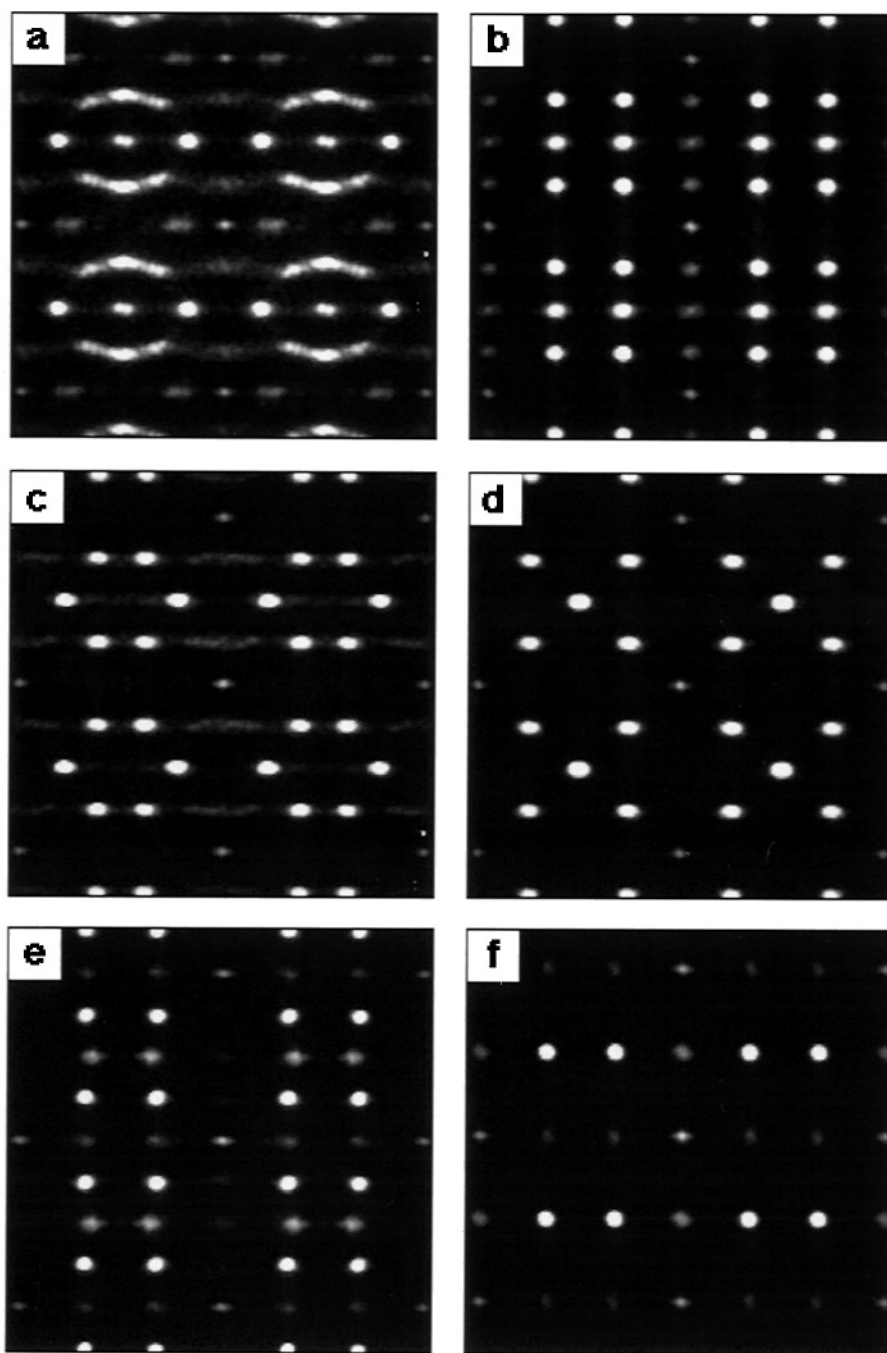
FIG. 6. Diffraction patterns corresponding to calculated images of Fig. 5. (a) η'-Cu$_6$Sn$_5$, (b) η^6-Cu$_5$Sn$_4$, (c) η^8-Cu$_5$Sn$_4$, (d) γ^4-Ni$_7$Ge$_4$, (e) Ni$_5$Ge$_3$, (f) Ni$_{17}$Ge$_{12}$.

γ^4-Ni$_7$Ge$_4$ at $x = 0.5$. The "checkerboard" structure that resulted was well-ordered, with a marked antiphase domain structure. It is not known from the experimental systems.

Diffuse-Scattering Superstructures

All the foregoing ordering patterns give rise to reasonably sharp superlattice reflections and only very weak streaking.

This is in contrast to the observed behavior of the Co–Ge, Co–Sn, and Ni–Sn systems, where undulating, continuous diffuse streaks trending along $\mathbf{z}^*$ dominate the diffraction patterns. Trial and error verified that these streaks broke up into discrete spots unless the interactions E_{i0} were kept very small. A systematic survey of the effects of "diagonal" interactions with $i \neq j \neq 0$ showed that although terms such as E_{21} and E_{31} do not play an important role in determining
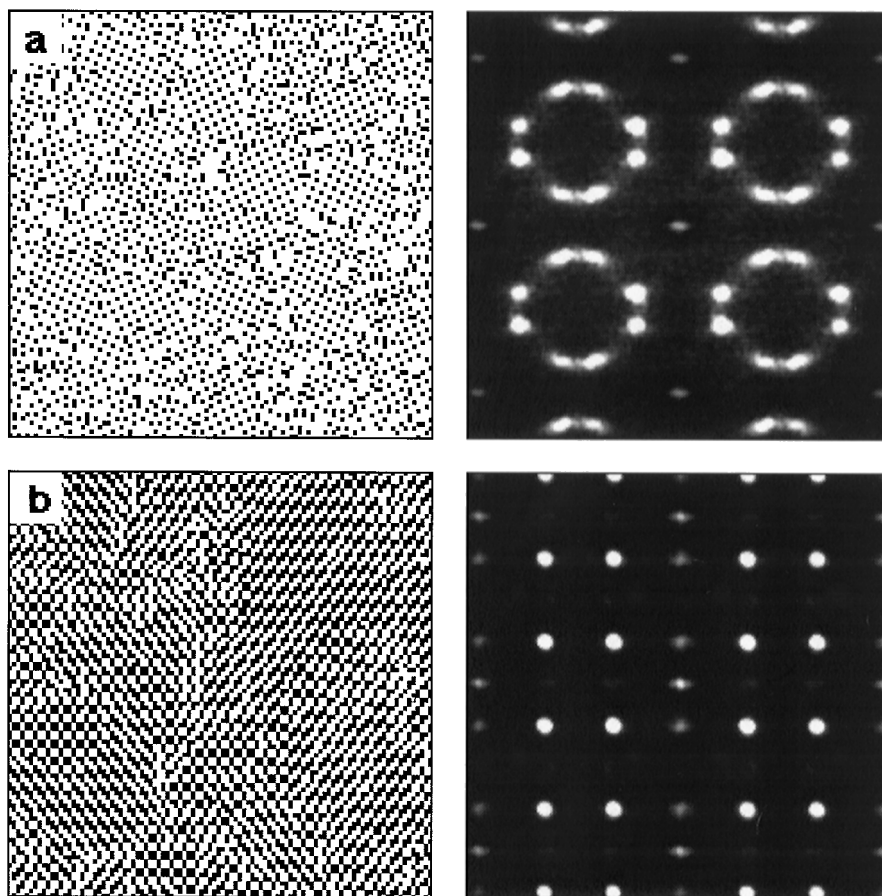
FIG. 7. Improved images (left) and diffraction patterns (right) for (a) η'-Cu_6Sn_5 and (b) $Ni_{17}Ge_{12}$ with E_{ij} modified as shown in third and fourth columns of Table 3.

the commensurate ordering patterns, these terms were important for the establishment of sinusoidal streaks. The best undulatory streaks were obtained for the E_{ij} values in the last column of Table 3. The composition used was $x = 0.333$ (equivalent to $x = 0.667$). The corresponding image and diffraction pattern are shown in Fig. 9a. Note the lack of perceptibly consistent modulation in the image. The diffraction pattern is almost identical to those found at the high-x end of the Ni–Sn system and to those of rapidly quenched Co–Sn alloys, in that the maximum and minimum values of h are $h_1 \approx \frac{1}{3}$ and $h_2 \approx \frac{1}{4}$, respectively. The streaking proved very sensitive to the relative magnitudes of the different E_{ij}, in that change of any of the first-nearest-neighbor E_{ij} by one unit of kT was sufficient to condense much of the diffuse intensity into spots. Generation of continuous loci of diffuse scattering by use of a small number of two-point interactions appears to be unusual. A more complex, two-dimensional pattern of "bicycle chain" diffuse streaks like those of this paper was successfully simulated by Welberry and Withers (13) using superposition of modulation waves.

Attempts to vary h_1 and h_2 by changing the interaction parameters met with limited success. Making E_{21} more negative $(-2, 0)$ appeared to increase h_1 to $\frac{1}{2}$ and h_2 to $\frac{1}{3}$ similar to those for $x = 0.67$ in the Co–Ge system but also concentrated much of the intensity near $l = 1$, which corresponded to islands of γ'-Co_3Sn_2 structure in the real space ordering pattern. Decreasing E_{01} to zero reduced the size of these and gave the ordering pattern and diffuse scattering seen in Fig. 9b. The diffraction pattern is very similar to the experimental one from $Co_{1.86}Ge$. It has not yet proved possible to simulate the double-sinusoidal streaking observed for high-x members of the Ni–Ge system, but the readiness with which multiphase intergrowths formed in the simulations of this paper (cf. Figs. 6f and 8c) suggests that this aim is achievable.

DISCUSSION AND CONCLUSIONS

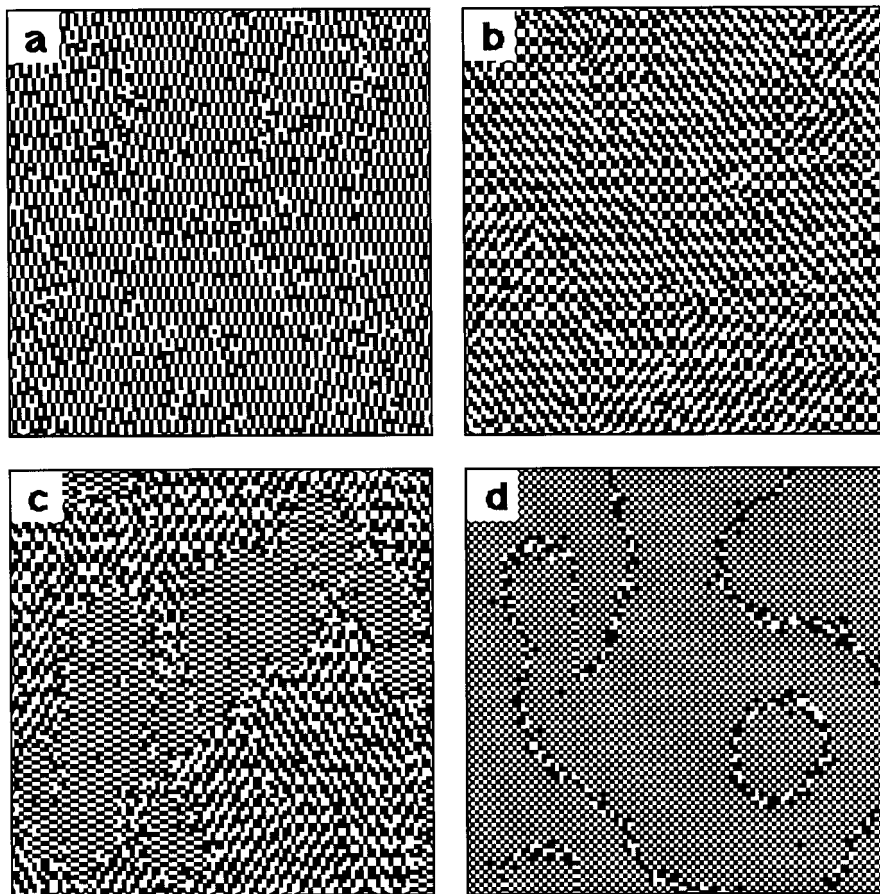Interactions more distant than second-nearest neighbor do not appear to be important in determining the A'

FIG. 8. Calculated images for $x = 0.5$, but using the E_{ij} appropriate for (a) η'-Cu$_6$Sn$_5$, (b) η^6-Cu$_5$Sn$_4$, (c) η^8-Cu$_5$Sn$_4$, and (d) γ^4-Ni$_7$Ge$_4$.

ordering patterns for the commensurate superstructures in the (Co, Ni, Cu)(Sn, Ge) $B8$-type alloys. The interactions E_{1j} ($j \neq 0$) and E_{i1} ($i \neq 0$) are not important in the commensurate phases, but those with $j = 1$ do play a role in the generation of ordering schemes that give sinusoidal diffuse streaks in diffraction. The superstructure generated (in systems that exhibit long-range order) is largely determined by just the three parameters E_{22}, E_{23}, and E_{30}, which vary widely from structure to structure. Negative E_{30} is associated with stabilizing a "honeycomb" ordering scheme of the majority substitutent in (001) layers. It is unclear why the other two second-nearest-neighbor interactions are so important. The axial interactions E_{0j} and E_{i0} are otherwise positive, except for E_{04}, a negative value of which helps to stabilize structures with period $2c$.

Some general trends with composition are apparent in systems that contain commensurate superstructures. In the Ni–Ge phases, there is a general trend of E_{23} and E_{30} becoming more positive as x increases. E_{22} is small over most of the composition range. The double set of diffuse streaks observed for large x pass through $(\frac{1}{4}\frac{1}{4}\frac{1}{2})$ and $(\frac{3}{8}\frac{3}{8}\frac{1}{2})$ approximately, which suggests that domains are present in

which E_{22} is more negative (γ^4-like local structure) and more positive (η^8-like), respectively.

Positive E_{22} is characteristic of the η^8-Cu$_5$Sn$_4$ and γ'-Co$_3$Sn$_2$ structures. It is noteworthy that the E_{ij} appropriate to the η^8 phase give rise to crystallites of the γ' phase if run for $x = 0.5$. These phases appear to be energetically related to one another but quite different from most of the phases of the Ni–Ge system. Conversely, the high-temperature η^6-Cu$_5$Sn$_4$ is stabilized by small E_{22}, E_{23}, and negative E_{30}, in which respect it resembles the low-x end of the Ni–Ge system. However, the need for a large positive C_{02} correlation requires small or zero E_{01} and E_{03} for the Ni$_{17-19}$Ge$_{12}$ structure.

The η'-Cu$_6$Sn$_5$ structure is energetically quite distinct from all the rest in that ordering on this pattern requires E_{04}, E_{11}, E_{22}, E_{23}, and E_{30} all to be highly positive. Its correspondent for $x = 0.5$ also appears quite different from any other structure generated.

Overall, there is tendency for E_{30} to become more negative, stabilizing the honeycomb ordering pattern, at higher temperatures and compositions near or within $x = 0.333$–0.667, with E_{23} varying in an antipathetic fashion.
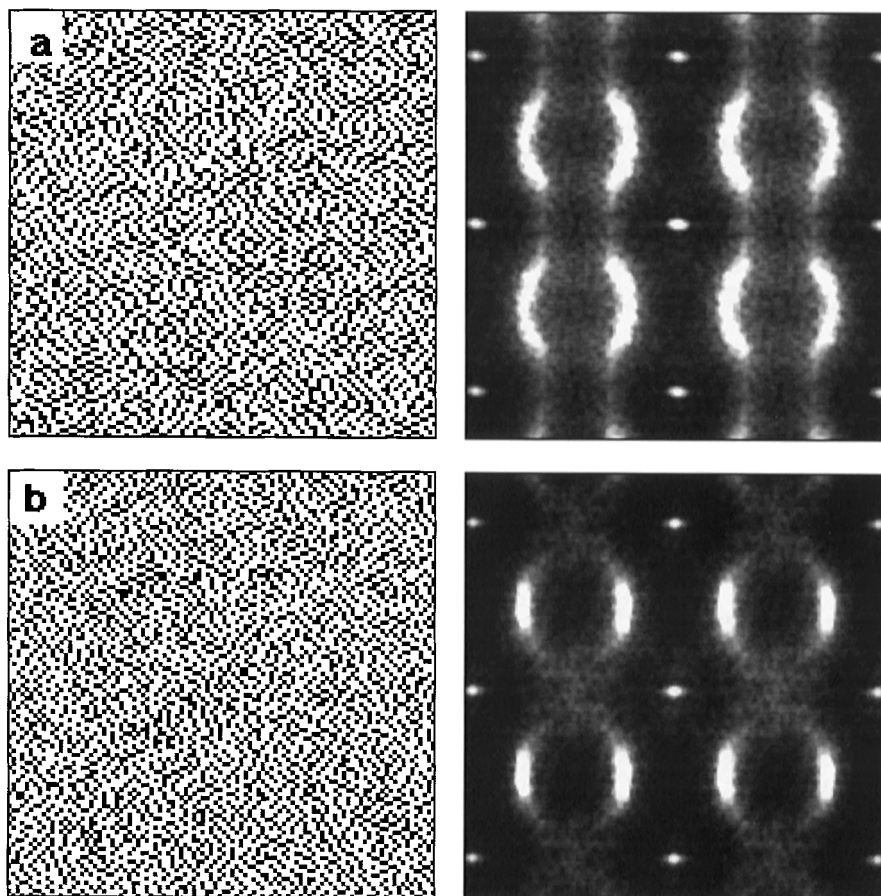
FIG. 9. Image (left) and diffraction pattern showing undulatory streaks (right) for (a) the E_{ij} in the penultimate column of Table 2 and $x = 0.333$ and (b) using E_{ij} in the last column of Table 2.

The nearly continuous sinusoidal streaking observed in the Ni–Sn and Co-bearing systems requires very small values for all the E_{0j} terms and relatively significant nonzero E_{21} and E_{31}. The sharpness of the streaks in the $(1\bar{1}0)^*$ direction implies that E_{i0} interactions remain large, however.

REFERENCES

1. S. Lidin and A.-K. Larsson, *J. Solid State Chem.* **118,** 313 (1995).
2. A.-K. Larsson, "Crystal structures of tin intermetallics; honeycomb nets, superstructures and Edshammar polyhedra," University of Lund, Lund, Sweden, 1994. [Ph.D. Thesis]
3. L.-E. Edshammar, "X-ray studies on binary alloys of aluminium with platinum metals," University of Stockholm, Stockholm, Sweden, 1969. [Ph.D. Thesis]
4. A.-K. Larsson, L. Stenberg, and S. Lidin, *Acta Crystallogr.*, *Sect. B: Struct. Sci.* **B50,** 636 (1994).
5. A.-K. Larsson, R. L. Withers, and L. Stenberg, *J. Solid State Chem.* **127,** 222 (1996).
6. A.-K. Larsson, and R. L. Withers, *J. Alloys Compd.*, in press.
7. P. Brand, *Z. Anorg. Allg. Chem.* **353,** 270 (1967).
8. A.-K. Larsson, L. Stenberg, and S. Lidin, *Acta Chem. Scand.* **49,** 800 (1995).
9. M. Ellner, T. Gödeke, and K. Schubert, *J. Less-Common Met.* **24,** 23 (1971).
10. A.-K. Larsson, L. Stenberg, and S. Lidin, *Z. Kristallogr.* **210,** 832 (1995).
11. B. D. Butler and T. R. Welberry, *J. Appl. Crystallogr.* **25,** 391 (1992).
12. T. R. Welberry and R. L. Withers, *J. Appl. Crystallogr.* **24,** 18 (1991).
13. T. R. Welberry and R. L. Withers, *J. Appl. Crystallogr.* **20,** 280 (1987).